

Article

# Design and Synthesis of an Eu-Based $\beta$ -Diketone-Sensor for the Detection of $\text{Al}^{3+}$ Ions

Guang Yu <sup>1</sup>, Yanjun Hou <sup>1,\*</sup>, Jinyuan Bai <sup>1</sup>, Haifeng Shao <sup>1</sup> and Haijun Niu <sup>1,2,\*</sup>

<sup>1</sup> School of Chemistry and Materials Science, Heilongjiang University, Harbin 150080, China; 13845184182@163.com (G.Y.); baijinyuanNO1@163.com (J.B.); 18088701791@163.com (H.S.)

<sup>2</sup> Key Laboratory of Chemical Engineering Process and Technology for High-efficiency Conversion, College of Heilongjiang Province, Harbin 150080, China

\* Correspondence: houyj@hlju.edu.cn (Y.H.); haijunniu@hotmail.com (H.N.); Tel.: +86-451-8660-9135 (Y.H. & H.N.)

Academic Editors: Mei Pan and Helmut Cölfen

Received: 28 March 2017; Accepted: 22 May 2017; Published: 23 May 2017

**Abstract:** A new  $\beta$ -diketone, 2,2,2-trifluoro-1-(4-hydroxy-2H-chromen-3-yl)ethanone (4-TFC), which contains a trifluorinated alkyl group and a rigid chromanone, has been designed and synthesised successfully, and utilized for the synthesis of a new stable  $\text{Eu}^{3+}$  ion-based 4-TFC lanthanide complex (1). The central  $\text{Eu}^{3+}$  ion is eight-coordinated by two O/N atoms from ancillary ligands and six oxygen atoms provided by three 4-TFC ligands. In particular, the complex (1) can detect  $\text{Al}^{3+}$  ions with high selectivity and sensitivity in a moment and can be seen by the naked eye clearly under 365 nm. The experimental data can be explained with the calculated transitions quite well.

**Keywords:** europium complex; fluorescence; detection; density functional theory (DFT) computation

## 1. Introduction

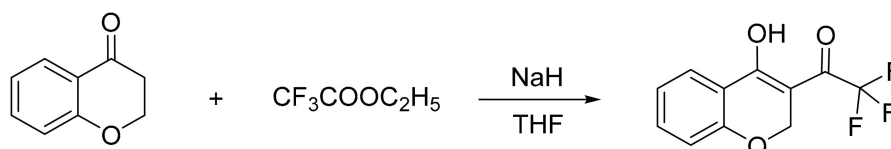
There are plenty of demands for novel fluorescent probes in the detection of metal ions because of their threat to human health and environment [1–6]. Among these, a common example is the presence of aluminum in food additives. Millions of people in the world are suffering from senile dementias. Scientists have found that Alzheimer’s disease and aluminum are closely related [7]. Also, they have found that aluminum causes damage in the human brain, heart, liver, kidney, and DNA [8]. Among the detection technologies, fluorometric methods have inspired an unprecedented wave of interest, not only in view of their structural diversity and aesthetic appeal, but also due to their distinguishing advantages, i.e., selectivity and non-invasiveness, high sensibility, easy operation, simplicity, short response time, and visualization [9–12]. Luminescent lanthanide complexes on the basis of  $\beta$ -diketones can generate strong luminescent signals with visible emission colors, which means that these types of complexes can be developed as promising chemical sensors [13,14]. The  $\beta$ -diketone ligand class is developing as one of the crucial “antennas” according to high harvest emissions by reason of the effectiveness of the energy transfer from this type of ligand to metal ions [15–17]. Following this idea,  $\text{Eu}^{3+}$  and 2,2,2-trifluoro-1-(4-hydroxy-2H-chromen-3-yl) ethanone (4-TFC) were chosen for the synthesis of a  $\beta$ -diketone complex in order to achieve the transition metal ion  $\text{Al}^{3+}$  based on the following reasons. (i) The coordination geometries of the transition metal ions always can be predicted, which is the decisive factor in designing the expected complexes with significant properties [18,19]; (ii) The 4-TFC ligand with low symmetry can increase the structural complexity, which promotes the synthesis of the complex [20]; (iii) The lanthanide complexes exhibit bright photoluminescence upon excitation in ligand-centered absorption bonds, and the process of detection is clearly visible under 365 nm [21,22].

In previous studies, Pradyut Ghosh [23] and Chen Yu-Chie [24] developed related substances for detecting  $\text{Al}^{3+}$  which have excellent properties. Probe 1H was synthesized by Pradyut Ghosh; its detection limit can be achieved at 0.5 nM. Glutathione-capped gold nanoclusters were fabricated by Yu-Chie Chen; they can detect  $\text{Al}^{3+}$  at 100 nM in water within 10 min. Compared with these substances, our complex is different in that it contains lanthanide metal ions  $\text{Eu}^{3+}$  which have high thermal stability (Figure S6) even when changed under fluorescence color from red to bright blue in seconds (Figure S10). We tested five varieties of vermicelli in order to detect their  $\text{Al}^{3+}$  content by using complex 1, and the results corresponded well with ICP tested. Moreover, the detection speed of complex 1 was very fast and the fluorescence phenomenon was easy to observe under 365 nm by the naked eye. The remarkable luminescence properties reveal that this complex could be an effective sensor for  $\text{Al}^{3+}$  ions. The absorptions of Eu and Al complexes were calculated with the time-dependent density functional theory (TD-DFT). The methods and calculations support the experimental data and explain them clearly.

## 2. Results and Discussion

### 2.1. Synthesis of 2,2,2-Trifluoro-1-(4-hydroxy-2H-chromen-3-yl)ethanone (4-TFC)

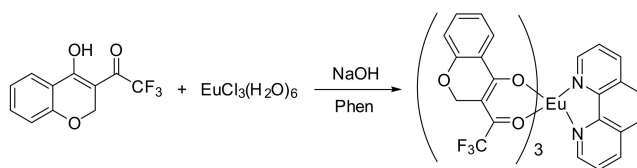
As shown in Scheme 1, 4-chromanone and ethyl trifluoroacetate were added into THF, and the mixed solution was stirred for 30 min. To this solution, NaH was added under an inert atmosphere and stirred for 24 h at room temperature. The reaction mixture was cooled to room temperature, then poured into ice water and acidified to pH 2–3 using hydrochloric acid (2 M). The final mixture was filtered and dried in a vacuum. Recrystallization from petroleum ether gave green flake crystals (2.6 g, 79%) (Figure S1). Elemental analysis (%) calcd for  $\text{C}_{11}\text{H}_7\text{F}_3\text{O}_3$  (244.17): C, 54.06; H, 2.87. Found: C, 54.04; H, 2.28. IR (KBr,  $\text{cm}^{-1}$ ): 2924 (w), 1611 (s), 1555 (w), 1484 (m), 1299 (w), 1237 (m), 1181 (m), 1142 (s), 1031 (w), 992 (m), 782 (m), 762 (m), 716 (w), 602 (s), 528 (w). (Figure S2).  $^1\text{H}$  NMR (400 MHz, DMSO)  $\delta$  = 7.83 (d,  $J$  = 6.8, 1H), 7.66 (t,  $J$  = 7.1, 1H), 7.18 (t,  $J$  = 7.5, 1H), 7.08 (d,  $J$  = 8.4, 1H), 5.09 (s, 2H). (Figure S3). ESI-TOF  $m/z$  = 244 ( $\text{M}^-$ ) (Figure S4).



Scheme 1. Synthesis of the ligand 4-TFC.

### 2.2. Synthesis of $\text{Eu}(4\text{-TFC})_3(\text{phen})$ (1)

The ligand 4-TFC was synthesized, as shown in Scheme 2. It was prepared by stirring solutions of 4-TFC. Then, NaOH was added to  $\text{CH}_3\text{OH}$  for 30 min. To this methanol solution,  $\text{EuCl}_3 \cdot 6\text{H}_2\text{O}$  was added dropwise, and the mixture was stirred for 24 h at room temperature. Then, two molar nitrogen donors were added into this solution for 10 h at 65 °C. Finally, 200 mL water was added to this mixture, and the precipitate thus formed was filtered, washed with water, and dried in the air. Single crystals were obtained in about one week by recrystallization from DCM/hexane.  $\text{Eu}(4\text{-TFC})_3(\text{phen})$  was achieved with a yield: 86%. Elemental analysis (%) calcd for  $\text{C}_{45}\text{H}_{26}\text{EuF}_9\text{N}_2\text{O}_9$  (1061.65): C, 50.91; H, 2.47; N, 2.64 Found: C, 51.23; H, 2.38; N, 2.51. IR (KBr)  $\nu_{\text{max}}$ : 1632  $\text{cm}^{-1}$  (s,  $\nu_{\text{C=O}}$ ), 1316  $\text{cm}^{-1}$  (s), 1258  $\text{cm}^{-1}$  (s), 1137  $\text{cm}^{-1}$  (s,  $\nu_{\text{C-F}}$ ), 763  $\text{cm}^{-1}$  (m,  $\nu_{\text{CF}_3}$ ) (Figure S5).



**Scheme 2.** Synthesis of the complex  $\text{Eu}(4\text{-TFC})_3(\text{phen})$ .

### 2.3. X-ray Crystallography

The single crystal X-ray structural analysis revealed that complex 1 crystallizes in the orthorhombic space group  $Pbca$  and the asymmetric unit of 1 consists of one europium (III) atom, one 1,10-phen ligand and three 4-TFC ligands. As shown in Figure 1, the Eu1 atom is coordinated by six  $\beta$ -diketone oxygen atoms, Eu1–O2 2.366(3) Å, Eu1–O3 2.355(3) Å, Eu1–O5 2.311(3) Å, Eu1–O6 2.380(3) Å, Eu1–O8 2.347(3) Å, and Eu1–O9 2.389(3) Å, from three 4-TFC ligands and two nitrogen atoms, Eu1–N1 2.585(3) Å and Eu1–N2 2.595(3) Å, from one 1,10-phen ligand to build a distorted hexahedron coordination geometry. The crystal data and refinement details are summarized in Table 1.

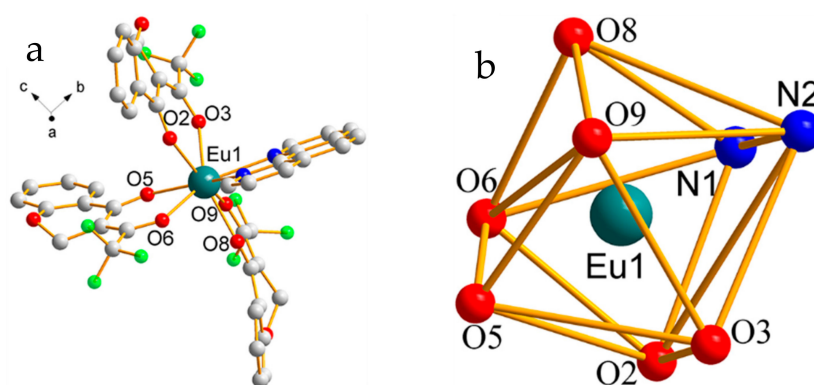


**Figure 1.** (a) Molecular structure of complex 1. (All hydrogen atoms have been omitted for clarity); (b) Coordination geometry of  $\text{Eu}^{3+}$  ion.

**Table 1.** Relevant crystal data for ligand 4-TFC and complex  $\text{Eu}(4\text{-TFC})_3(\text{phen})$ .

Empirical Formula	$\text{C}_{45}\text{H}_{26}\text{EuF}_9\text{N}_2\text{O}_9$	$\text{C}_{11}\text{H}_7\text{F}_3\text{O}_3$
Formula weight	1061.64	244.17
Color	Colorless	Green
Cryst syst	Orthorhombic	Monoclinic
Space group	$Pbca$	$P2_1/c$
Temperature (K)	293(2) K	293(2) K
a (Å)	20.5707(18)	11.927
b (Å)	19.0486(17)	7.523
c (Å)	21.4827(19)	13.044
$\alpha$ (deg)	90	90
$\beta$ (deg)	90	119.09
$\gamma$ (deg)	90	90
V (Å <sup>3</sup> )	8417.8(13)	1022.8
Z	8	4
$\rho$ (g cm <sup>−3</sup> )	1.675	1.586
$\mu$ (mm <sup>−1</sup> )	1.590	0.150
F (000)	4208	496
R <sub>1</sub> [ $I > 2\sigma(I)$ ]	0.0393	0.0478
wR <sub>2</sub> [ $I > 2\sigma(I)$ ]	0.0966	0.1347
R <sub>1</sub> (all data)	0.06371	0.0715
wR <sub>2</sub> (alldat)	0.1129	0.1555
GOF on F <sup>2</sup>	1.097	1.015
CCDC	1443763	1524762

#### 2.4. UV-Vis Spectra Analysis

The ultraviolet-visible (UV-Vis) absorption spectra of the ligand 4-TFC and the complex  $\text{Eu}(4\text{-TFC})_3(\text{phen})$  were measured in DMF solution at the concentration of  $1 \times 10^{-5}$  mol/L in the range of 200–450 nm at room temperature. Figure 2 shows that the maximum UV-Vis absorption for 4-TFC is at a wavelength of 360 nm, attributed to the singlet–singlet  $\pi\text{-}\pi^*$  transition of the aromatic rings. Compared with the maximum absorption wavelength of 4-TFC, the maximum absorption wavelength of  $\text{Eu}(4\text{-TFC})_3(\text{phen})$  is around 365 nm, in which the maximum absorption wavelength undergoes a red-shift from 360 nm to 365 nm, attributed to the perturbation of the  $\text{Eu}^{3+}$  ion. Meanwhile, with the maximum absorption band of 4-TFC and  $\text{Eu}(4\text{-TFC})_3(\text{phen})$  at 360–365 nm, we can reasonably infer that the  $\text{Eu}^{3+}$  ion of the complex has almost no influence on the singlet excited state of the ligand. The absorption intensity of the complex is about three times as great as the ligand in the UV-Vis spectra at the concentration of  $1 \times 10^{-5}$  mol/L. This result agrees well with the presence of three ligands in each complex.

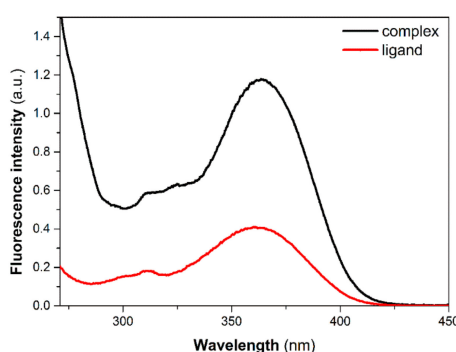


**Figure 2.** UV-Vis absorption spectra of 4-TFC and complex  $\text{Eu}(4\text{-TFC})_3(\text{phen})$  in DMF ( $c = 1 \times 10^{-5}$  mol/L).

#### 2.5. Excitation Spectra and Emission Spectra

Figure 3 shows the excitation spectra and emission spectra of complex  $\text{Eu}(4\text{-TFC})_3(\text{phen})$ . The excitation wavelength at 360 nm is mainly attributed to the singlet–singlet  $\pi\text{-}\pi^*$  electron transition of 4-TFC ligand. The emission spectra of complex  $\text{Eu}(4\text{-TFC})_3(\text{phen})$  lying in the range of 550–700 nm coincide with the characteristic emission bands of the  $\text{Eu}^{3+}$  ions corresponding to the  ${}^5\text{D}_0 \rightarrow {}^7\text{F}_j$  ( $J = 0\text{--}4$ ) transitions. Among these, the strongest emission is at  $\lambda = 612$  nm for the electric dipole transition  ${}^5\text{D}_0 \rightarrow {}^7\text{F}_2$ , and its corresponding intensity is very sensitive and easy to change as the coordination environment changes. This very intense  ${}^5\text{D}_0 \rightarrow {}^7\text{F}_2$  peak is responsible for the brilliant red emission of the complex, which indicates the presence of a single major chemical environment around the  $\text{Eu}^{3+}$  ion.

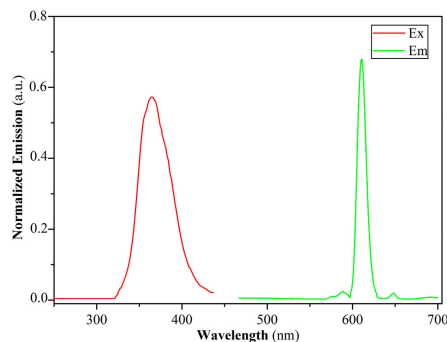


**Figure 3.** Excitation (red line) and emission spectra (green line) of complex 1 (excited and monitored at 324 and 612 nm, respectively).

## 2.6. Luminescent Properties

In order to explore the sensing ability of complex 1 through its luminescence, a solution ( $1 \times 10^{-2}$  mol/L) of complex 1 was added into DMF including  $\text{Na}^+$ ,  $\text{Fe}^{3+}$ ,  $\text{Ga}^{3+}$ ,  $\text{Cr}^{3+}$ ,  $\text{K}^+$ ,  $\text{Ag}^+$ ,  $\text{Mg}^{2+}$ ,  $\text{Mn}^{2+}$ ,  $\text{Ni}^{2+}$ ,  $\text{Pb}^{2+}$ ,  $\text{Zn}^{2+}$ , and  $\text{Cd}^{2+}$  (molar ratio 1:2) (Figure 4), respectively. Every  $\text{M}(\text{NO}_3)_x$  in DMF was sonicated for 20 min to ensure that the metal ions were homogeneous in the solution before being detected. Competitive  $\text{Al}^{3+}$  metal ions were selected for quenching the luminescence in seconds, while other metal ions showed no distinct interference with the emission by the displayed luminescence. The individual effects on the emission of luminescence between  $\text{Al}^{3+}$  and  $\text{M}^{x+}$  ions indicate that complex 1 can be regarded as a promising luminescent probe for  $\text{Al}^{3+}$  ions.

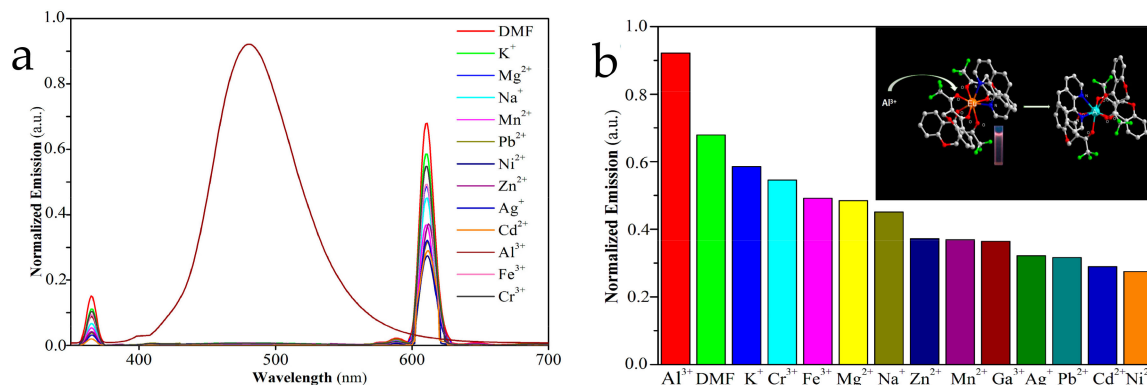


**Figure 4.** (a) Luminescence spectra of complex 1 and (b) the corresponding luminescence intensity of complex 1 with the indicated metal ions in DMF solution ( $c = 1 \times 10^{-2}$  mol/L $^{-1}$ ).

Exploring the influence level of different competitive metal ions ( $\text{Na}^+$ ,  $\text{Fe}^{3+}$ ,  $\text{Ga}^{3+}$ ,  $\text{Cr}^{3+}$ ,  $\text{K}^+$ ,  $\text{Ag}^+$ ,  $\text{Mg}^{2+}$ ,  $\text{Mn}^{2+}$ ,  $\text{Ni}^{2+}$ ,  $\text{Pb}^{2+}$ ,  $\text{Zn}^{2+}$  and  $\text{Cd}^{2+}$ ) on the luminescence intensities could be considered a significant part in the process of checking the specificity of complex 1 towards  $\text{Al}^{3+}$  ions. The experimental results shown in Figure 5 reveal that complex 1 still maintains a high degree of selectivity towards  $\text{Al}^{3+}$  ions, and the presence of other metal ions do not have an effect on the detection of  $\text{Al}^{3+}$  ions by complex 1. The detection speed is still in the range of seconds. A wide range of blue shift in fluorescence spectra and an obvious color conversion from red to blue were observed in DMF solution gave a better understanding of the selective ability of complex 1. With confidence in these indicative results, we can draw the conclusion that complex 1 is an effective fluorescent sensor for the selective detection of  $\text{Al}^{3+}$  ions in DMF solution.

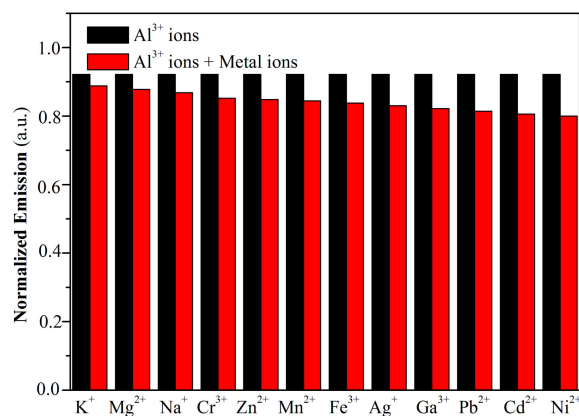


**Figure 5.** Fluorescence influence of various competing metal ions compared to  $\text{Al}^{3+}$  ions in DMF solution. The black bars represent only  $\text{Al}^{3+}$  ions in DMF ( $c = 1 \times 10^{-2}$  mol/L). The red bars represent the fluorescence intensity after adding the corresponding competing metal ions.

The concentration of  $\text{Al}^{3+}$  ions towards the luminescence intensity was further investigated in DMF under 365 nm. To investigate the fluorescent conversion process of  $\text{Al}^{3+}$  ions from unequal concentration, complex 1 was dispersed in different concentrations of  $\text{Al}^{3+}$  ions in DMF solution. As illustrated in Figure 6, the luminescence intensity increased gradually with the increase of the concentration until a saturation point was reached. Furthermore, the luminescence intensity of complex 1 in different concentrations of  $\text{Al}^{3+}$  ions could be clearly observed in the absorption spectrum, until the probe reached a concentration less than  $2 \times 10^{-6}$  mol/L.

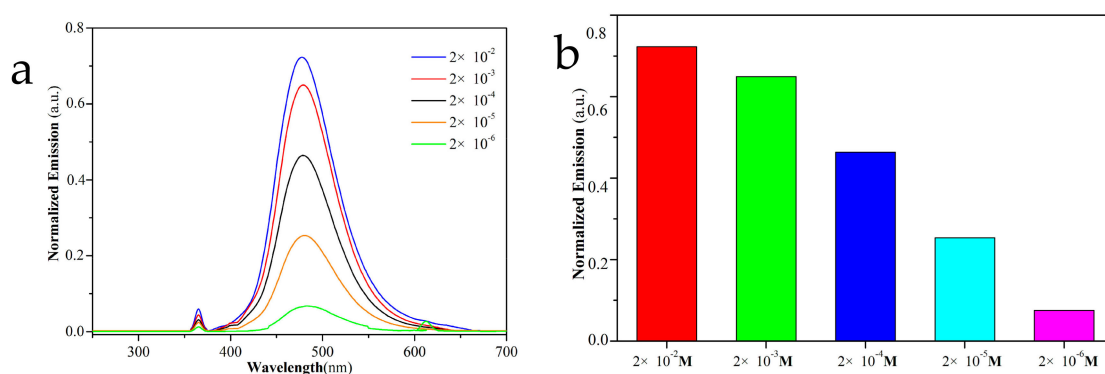


**Figure 6.** (a) Luminescence spectra of complex 1 and (b) the corresponding luminescence intensity of complex 1 in solutions with different concentrations of  $\text{Al}^{3+}$  ions.

We purchased five kinds of vermicelli from different street hawkers to be used as samples for detecting  $\text{Al}^{3+}$ . These vermicelli samples had not been tested by the Food Safety Authority. Every 1.000 g sample after drying was treated with hydrogen peroxide and concentrated nitric acid in Teflon cans. The Teflon beaker was gently shaken to ensure that the sample was well dispersed. Then, the sample was placed in a microwave digestion device and digested for 30 min at 180 °C. After completely cooling, the solution was removed and transferred into a 100-mL volumetric flask, diluted with water to a total volume of 100 mL, and mixed well [25]. The solution was then diluted 20 times with water. Sample 6 was the control group, which only contained  $2 \times 10^{-6}$  mol/L  $\text{Al}^{3+}$  ion solution, and was limited to contain no more than  $1.85 \times 10^{-6}$  mol/L  $\text{Al}^{3+}$  after our digestion procedure by the Chinese Food Safety Authority. (It must be pointed out that the concentration is limited to no more than  $3.70 \times 10^{-6}$  mol/L under normal conditions, but in order to achieve a color change we had to reach the detection limit of  $2 \times 10^{-6}$  mol/L of complex 1). We used complex 1 to detect the remaining samples in the color tube. After adding the complex to samples 2 and 6, there was an obvious color conversion from red to blue under 365 nm. At the same time, the quantitative analysis of  $\text{Al}^{3+}$  of the five types of vermicelli was performed by ICP-MS analysis using the standard method [26]. The results of the ICP-MS analysis are shown in Table 2. All samples were tested at least three times and averages are reported.

**Table 2.** The contents of  $\text{Al}^{3+}$  ions in vermicelli detected by ICP-MS.

Sample	Color	Diameter (mm)	Concentration (mol/L)	After Adding Complex 1 (365 nm)
Sample 1	gray	1.4	$0.81 \times 10^{-6}$	red
Sample 2	translucent	2.9	$5.10 \times 10^{-6}$	red to blue
Sample 3	gray	3.3	$1.21 \times 10^{-6}$	red
Sample 4	gray	1.8	$0.58 \times 10^{-6}$	red
Sample 5	translucent	2.8	$1.27 \times 10^{-6}$	red
Sample 6	—	—	$2.00 \times 10^{-6}$	red to blue
water	—	—	—	red

For the detection of metal ions, an  $\text{Eu}(4\text{-TFC})_3(\text{phen})$  probe was used to detect  $\text{Al}^{3+}$  ion selectively. In parallel, a series of methods for detecting were prepared under identical conditions to confirm if only  $\text{Eu}(4\text{-TFC})_3(\text{phen})$  has specific detection properties for  $\text{Al}^{3+}$  ions at the concentration of  $1 \times 10^{-2}$  mol/L, as shown in Figure 7 and Table 3. All of these (a–j) added the ligand into DMF firstly, and then added the metal ions into the corresponding solution. All solutions underwent a color conversion in seconds and the colors remained stably for a long time. Results of the experiments show that the ligand 4-TFC and the auxiliary ligand phen cannot have an effect on the detection of distinguishing  $\text{Al}^{3+}$  ions. However, the color of the light can be changed from red to blue rapidly by adding  $\text{Al}^{3+}$  ions into the solution of  $\text{Eu}(4\text{-TFC})_3(\text{phen})$ . Therefore, it is essential to synthesize the complex  $\text{Eu}(4\text{-TFC})_3(\text{phen})$  for detecting  $\text{Al}^{3+}$  ions. In addition, complex 1 displayed remarkable specificity toward acetone (Figures S7 and S8).

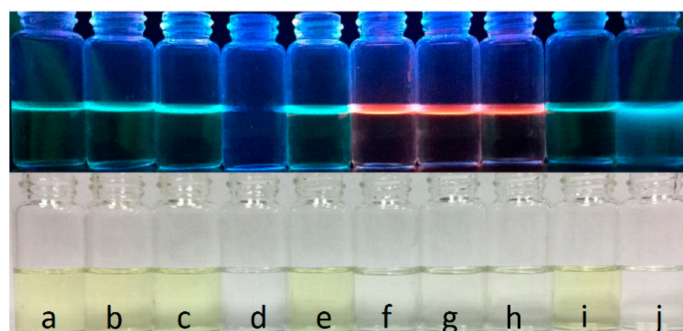


**Figure 7.** Different colors of the mixtures under 365 nm.

The ligand 4-TFC belongs to the  $\beta$ -diketone ligands, which is the first class of studied ligands. The advantage of these is that they are easier to synthesize and modify. In lanthanide  $\beta$ -diketone complexes, energy migration between chromophores and acceptors is a necessary procession in lighting, and the extensively accepted energy transfer mechanism is proposed by Crosby et al. In their complex, there is a high efficiency of energy transfer from the  $\beta$ -diketone ligand with a high absorption coefficient to  $\text{Eu}^{3+}$ . Thus, the complex has a very high luminous efficiency. Due to the existence of F ions that have high electronegativity in the functional group R, the sensitizing effect of  $\text{CF}_3$  in the terminal functional group R is the strongest. Generally, the sensitization pathway of the europium luminescence is an intramolecular energy transfer. The energy from the light source can cause ligands to transfer from a ground state to an excited singlet state, after an intersystem cross to the triplet state. Subsequently, the energy transfers from the triplet state to the  $^5\text{D}_j$  of the  $\text{Eu}^{3+}$  ions, then crosses the intersystem to the emitting  $^5\text{D}_0$  state. Finally, the  $\text{Eu}^{3+}$  ions emit when the ground state occurs.

**Table 3.** Different color of the mixture under 365 nm.

Sample	Complex	4-TFC	Phen	$\text{Eu}^{3+}$	$\text{Al}^{3+}$	Color
a		add				green
b		add			add	green
c		add	add		add	green
d			add		add	colorless
e		add		add		green
f			add	add		red
g		add	add	add		red
h			add	add	add	red
i		add		add	add	green
j	add					blue

## 2.7. Computational Studies

The optimized results of the geometry structures of complexes are presented in Figure 8 and Table 4. It is noted that the  $\text{Eu}^{3+}$  ion in the complex is ligated to six oxygen atoms from the three 4-TFC and two nitrogen atoms from 1,10-phenanthroline, resulting in a distorted square antiprism geometry. However, the  $\text{Al}^{3+}$  ion in the complex is ligated to six oxygen atoms from the three 4-TFC, forming a six-coordinated structure, and the 1,10-phenanthroline molecule is far away from the  $\text{Al}^{3+}$  ionic. The ionic radii of  $\text{Al}^{3+}$  ions is 0.535 Å, which is much smaller than the ionic radii of  $\text{Eu}^{3+}$  ions, 0.947 Å. It is clear that the affinity between O and Al atoms calculated from the bond dissociation energies is larger than that between O and Eu atoms. Resultingly, the Al atom is nearer to the O atoms in the Al complex than in the Eu complex. The bond lengths of the Al–O bonds are smaller than those of the Eu–O bonds, and the Al atoms are much closer to the O atoms than Eu atoms in the complex. As shown in Table 4, the bond lengths of the Al–O bonds in the range of 1.9003–1.9255 Å are shorter than those of the Eu–O bonds in the range of 2.3370–2.3964, which means the corresponding bonding strength of Al–O is much stronger than that of Eu–O in the complexes. That indicates that the  $\text{Eu}^{3+}$  ion can be replaced by the  $\text{Al}^{3+}$  ion easily during the ion determination.

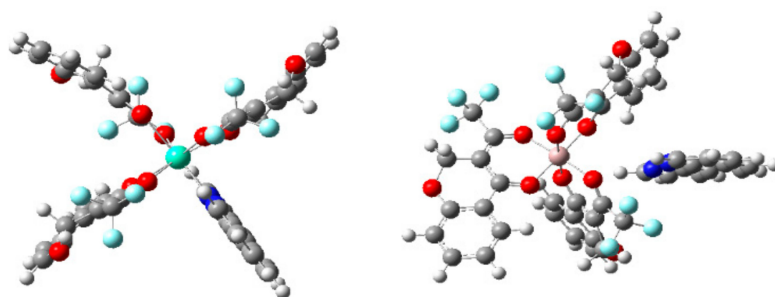


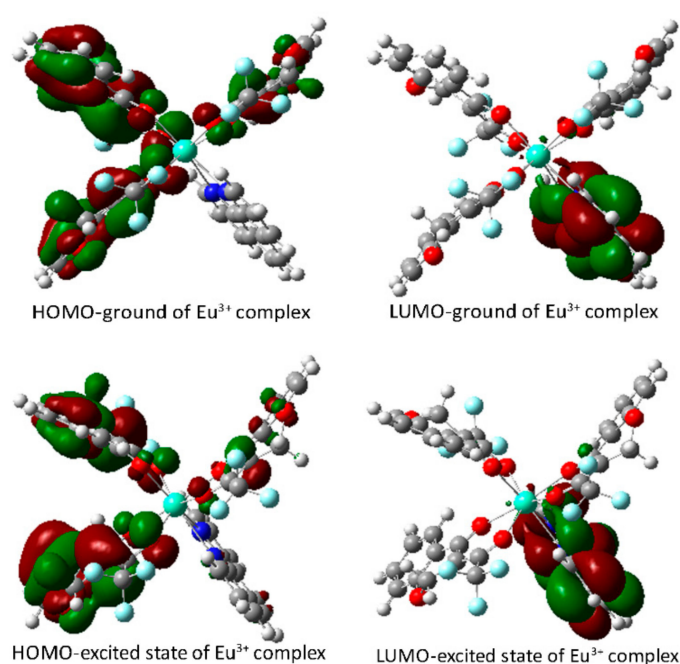
Figure 8. Optimized geometry structures of complexes ( $\text{Eu}^{3+}$  complex (left),  $\text{Al}^{3+}$  complex (right)).

Table 4. Selected bond length and angles for optimized geometry structures of complexes.

Bond Length (Å)	Bond Length (Å)	Bond Angles (°)	Bond Angles (°)
Eu(1)–O(2) 2.3761	Al(1)–O(2) 1.9136	O(2)–Eu(1)–O(3) 70.2499	O(2)–Al(1)–O(3) 89.9886
Eu(1)–O(3) 2.3813	Al(1)–O(3) 1.9189	O(5)–Eu(1)–O(6) 69.9090	O(5)–Al(1)–O(6) 89.1116
Eu(1)–O(5) 2.3845	Al(1)–O(5) 1.9226	O(8)–Eu(1)–O(9) 70.9363	O(8)–Al(1)–O(9) 90.0988
Eu(1)–O(6) 2.3783	Al(1)–O(6) 1.9255	N(1)–Eu(1)–N(2) 61.2205	N(1)–Al(1)–N(2) 31.6322
Eu(1)–O(8) 2.3964	Al(1)–O(8) 1.9003		
Eu(1)–O(9) 2.3370	Al(1)–O(9) 1.9193		
Eu(1)–N(1) 2.6966	Al(1)–N(1) 4.6949		
Eu(1)–N(2) 2.6852	Al(1)–N(2) 5.2663		

The results of the theoretical calculations for the absorption properties of the complexes are shown in Figure 9 and Figure S9 and Table 5. The HOMO and LUMO levels for the ground and singlet excited states of the  $\text{Eu}^{3+}$  complex were  $-0.21$  eV and  $-0.08$  eV,  $-0.31$  eV and  $0.05$  eV, respectively. The electronic cloud distribution of HOMO in the ground and singlet excited states localizes at the three 4-TFC group, while that of LUMO localizes at 1,10-phenanthroline. As shown in Table 5, the lowest excitation energy of the  $\text{Eu}^{3+}$  complex calculated by TD-DFT is 3.14 eV. The absorption transition is mainly due to the ligand-to-metal charge transfer (LMCT), metal-to-ligand charge transfer (MLCT), and metal-centered (MC) transitions. Other high-energy absorption transitions are mainly due to the intraligand charge transfer (ILCT or  $\pi \rightarrow \pi^*$ ), LMCT, MLCT, and MC transitions. In comparison with the absorption spectra of the  $\text{Eu}^{3+}$  complex, the lowest excitation energy of the  $\text{Al}^{3+}$  complex calculated by TD-DFT is 2.78 eV, which is mainly due to the ILCT, LMCT, and MLCT transitions. It is notable that the S9 high-energy absorption transitions are mainly due to LMCT and MLCT according to the

selected frontier molecular orbitals of the  $\text{Al}^{3+}$  complex, there is not ILCT transition in the absorption transitions (Figure S9).



**Figure 9.** The results of the theoretical calculations for the absorption properties of the complexes.

**Table 5.** Absorptions of Eu and Al complexes calculated with the TD-DFT method.

Complexes	Sn	Confign	CI Codff	E/nm (eV)	Oscillator	Assignment
Eu complex	S <sub>6</sub>	H-2 → L	0.2741	362.17 (3.14)	0.1253	LMCT/MLCT/MC
	S <sub>7</sub>	H-1 → L + 2	0.3350	276.44 (4.49)	0.2128	ILCT/LMCT/MLCT/MC
	S <sub>8</sub>	H → L + 3	0.2709	270.48 (4.58)	0.4099	ILCT/LMCT/MLCT/MC
	S <sub>9</sub>	H → L + 4	0.3649	269.09 (4.61)	0.3189	ILCT/LMCT/MLCT/MC
Al complex	S <sub>7</sub>	H-3 → L + 1	0.2465	446.62 (2.78)	0.1685	ILCT/LMCT/MLCT
	S <sub>8</sub>	H-4 → L6	0.4417	270.08 (4.59)	0.2344	ILCT/LMCT/MLCT
	S <sub>9</sub>	H-1 → L + 2	0.4838	266.22 (4.66)	0.4058	LMCT/MLCT

### 3. Materials and Instrumentation

$\text{Eu}_2\text{O}_3$  (99.99% purity) was purchased from Ji Nan Rare Earth Chemical Plant (Shandong, China). Sodium hydride (60%, A. R.) and 1,10-phenanthroline monohydrate (99%, A. R.) were bought from Sigma-Aldrich (Beijing, China). 4-chromanone and ethyl trifluoroacetate were obtained from Sun Chemical Technology (Shanghai, China) Co., Ltd.  $\text{EuCl}_3 \cdot 6\text{H}_2\text{O}$  was synthesized according to the literature by dissolving lanthanide oxide in a slight excess of hydrochloric acid. Other reagents and solvents were commercially available and used without further treatment. Fourier transform infrared (FT-IR) spectra were obtained on a Perkin-Elmer spectrometer. One spectrophotometer employed KBr disks in the range of 4000–400  $\text{cm}^{-1}$ . Ultraviolet (UV) spectra were recorded on a Perkin-Elmer Lambda 35 spectrometer. Thermal analysis was conducted on a Perkin-Elmer STA 6000 with a heating rate of 10  $^\circ\text{C min}^{-1}$  in a  $\text{N}_2$  temperature range from 30  $^\circ\text{C}$  to 800  $^\circ\text{C}$ .  $^1\text{H}$ NMR spectra were recorded on a Bruker Avance (III) 400 MHz spectrometer in DMSO solution. Excitation and emission spectra were measured by an Edinburgh FLS 920 fluorescence spectrophotometer. The data were analyzed by software supplied by Edinburgh Instruments. Diffraction intensity data were collected on a Bruker SMART APEX II X-ray diffractometer with graphite monochromated Mo  $\text{K}\alpha$  radiation ( $\lambda = 0.71073 \text{ \AA}$ ).

All the data were collected at a temperature of  $18 \pm 3$  °C. ICP-MS data were recorded on an ICP-MS Perkin Elmer SCIEX ELAN 5000.

APEX2 and SAINT programs [27,28] were used for preliminary determination, the determination of integrated intensities, and the unit cell refinement of the crystals. The structures were solved with SHELXS-2014/7 and refined with SHELXL-2014/7 [29].

All computations were performed using the Gaussian03 code [30]. The initial geometry of the  $\text{Al}^{3+}$  complex was obtained by replacing the  $\text{Eu}^{3+}$  ion with an  $\text{Al}^{3+}$  ion. The geometry structures in the ground and excited states were optimized with B3LYP functional (Becke's three-parameter nonlocal exchange functional) and unrestricted B3LYP (UB3LYP) methods, respectively. In the  $\text{Al}^{3+}$  complex calculations, the LANL2DZ basis sets with the effective core potentials (ECPs) of Hay and Wadt were used for Al atoms, and 6-31G(d) basis sets were used for other atoms. In the  $\text{Eu}^{3+}$  complex calculations, the ECP52MWB basis sets with the effective core potentials (ECPs) were used for Eu atoms, and 6-31G(d) basis sets were used for other atoms. Time-dependent density functional theory (TD-DFT) was employed to calculate the absorption properties on the basis of the optimized geometry structure in the excited states. The lowest spin-allowed singlet-singlet transitions, up to a wavelength of 245 nm, were taken into account while calculating the optical absorption spectra.

#### 4. Conclusions

In summary, we synthesized a new dual-functional  $\beta$ -diketonate ligand 4-TFC, incorporating a trifluorinated alkyl group, a rigid chromanone, and 1,10-phen. Further systematic investigations on the photophysical properties suggested that the designed  $\text{Eu}(4\text{-TFC})_3(\text{phen})$  complex is a sensitive and effective probe to sense metal cations and small molecules. DFT calculations suggested that the average bond length (Al–O) around aluminum in the resulting  $\text{Al}^{3+}$  complex is much smaller than the corresponding average bond length (Eu–O) of complex 1. The calculation data demonstrate that the  $\text{Eu}^{3+}$  ion can be replaced by the  $\text{Al}^{3+}$  ion easily during the ion determination [31,32]. The luminescence intensities of complex 1 plays an essential role in detecting the  $\text{Al}^{3+}$  ion. Moreover, complex 1 also shows strongly selective luminescence for acetone. Therefore, the newly-designed  $\beta$ -diketone 4-TFC europium complex may be useful in more realistic conditions in the future.

**Supplementary Materials:** The following are available online at [www.mdpi.com/2073-4352/7/6/150/s1](http://www.mdpi.com/2073-4352/7/6/150/s1), Figure S1: Molecular structure of ligand 4-TFC, Figure S2: IR of the ligand 4-TFC, Figure S3: HNMR of the ligand 4-TFC, Figure S4: Expanded regions of the ESI-TOF of 4-TFC, Figure S5: IR of the complex  $\text{Eu}(4\text{-TFC})_3(\text{phen})$ , Figure S6: Thermal gravimetric of complex  $\text{Eu}(4\text{-TFC})_3(\text{phen})$ , Figure S7: (a) Luminescence spectra of complex 1 and (b) the corresponding luminescence intensity of complex 1 with following organic pure solvents in DMF solutions ( $c = 1 \times 10^{-2}$  mol/L), Figure S8: Schematic energy level diagram and energy transfer process for complex 1. S1, first excited singlet state; T1, first excited triplet state, Figure S9: The results of theoretical calculations for absorption properties of the complexes, Figure S10: Effect of  $\text{Al}^{3+}$  concentration on fluorescence intensity in the presence of  $\text{Eu}^{3+}$ .

**Acknowledgments:** We are grateful for the financial support from the National Natural Science Foundation of China (No. 51373049) and the Education Department of Heilongjiang Province of China (No. 12521413).

**Author Contributions:** Guang Yu conceived and designed the experiments; Guang Yu performed the experiments; Yanjun Hou, Haijun Niu, Haifeng Shao and Jinyuan Bai analyzed the data; Yanjun Hou contributed reagents/materials/analysis tools; Guang Yu wrote the paper.

**Conflicts of Interest:** The authors declare no conflict of interest.

#### References

1. Zhao, J.; Wang, Y.N.; Dong, W.W.; Wu, Y.P.; Li, D.S.; Zhang, Q.C. A Robust Luminescent Tb(III)-MOF with Lewis Basic Pyridyl Sites for the Highly Sensitive Detection of Metal Ions and Small Molecules. *Inorg. Chem.* **2016**, *55*, 3265–3271. [[CrossRef](#)] [[PubMed](#)]
2. Zhao, X.L.; Tian, D.; Gao, Q.; Sun, H.W.; Xu, J.; Bu, X.H. A chiral lanthanide metal–organic framework for selective sensing of Fe(III) ions. *Dalton Trans.* **2016**, *45*, 1040–1046. [[CrossRef](#)] [[PubMed](#)]

3. Wang, L.; Qin, W.; Tang, X.; Dou, W.; Liu, W.; Teng, Q.; Yao, X. A selective, cell-permeable fluorescent probe for Al<sup>3+</sup> in living cells. *Org. Biomol. Chem.* **2010**, *8*, 3751–3757. [[CrossRef](#)] [[PubMed](#)]
4. Ashton, T.D.; Jolliffe, K.A.; Pfeffer, F.M. Luminescent probes for the bioimaging of small anionic species in vitro and in vivo. *Chem. Soc. Rev.* **2015**, *44*, 4547–4595. [[CrossRef](#)] [[PubMed](#)]
5. Muhammad, S.; Ki, H.L. Optical sensor: A promising strategy for environmental and biomedical monitoring of ionic species. *RSC Adv.* **2015**, *5*, 72150–72287. [[CrossRef](#)]
6. Marek, P.; Oksana, P.; Jerzy, K.; Alina, M.; Grzegorz, D.; Teresa, B.; Anna, M.K.; Rik, V.D. Highly photoluminescent europium tetraphenylimidodiphosphinate ternary complexes with heteroaromatic co-ligands. Solution and solid state studies. *J. Lumin.* **2016**, *170*, 411–419. [[CrossRef](#)]
7. Stephen, C.B. Low levels of aluminum can lead to behavioral and morphological changes associated with Alzheimer's disease and age-related neurodegeneration. *Neurotoxicology* **2016**, *52*, 222–229. [[CrossRef](#)]
8. Yahya, A.K.; Xinsen, S.; Timothy, J.P.; Mark, R.J.E.; Carl, R. Tetraphenolate niobium and tantalum complexes for the ring opening polymerization of epsilon-caprolactone. *Dalton Trans.* **2015**, *44*, 12349–12356. [[CrossRef](#)]
9. Paula, G.; Vladimir, M.A.; Victor, A.T.; Dagmara, K.; Janina, L. The ligand-to-metal energy transfer and the role of Lewis base ligands and silver plasmons in emission of new type of lanthanide phosphors. *J. Lumin.* **2016**, *170*, 340–347. [[CrossRef](#)]
10. Wen, J.Z.; Hai, Y.W. Preparation and luminescent properties of lanthanide (Eu<sup>3+</sup> and Tb<sup>3+</sup>) complexes grafted to 3-aminopropyltriethoxysilane by covalent bonds. *Opt. Mater.* **2015**, *50*, 208–214. [[CrossRef](#)]
11. Martín, R.P.; Martín, I.R.; Lahoz, P.; Hernández, N.S.; Pereira, S.P.S.; Hernández, I.; Lavín, V.; Ramos, S.M. An erbium(III)-based NIR emitter with a highly conjugated  $\beta$ -diketonate for blue-region sensitization. *J. Alloy Compd.* **2015**, *619*, 553–559. [[CrossRef](#)]
12. Wei, G.T.; Yi, N.X.; Jin, T.T.; Pei, Z.G.; Jin, H.D.; Xin, W.; Zhi, B.Z. Colorimetric and fluorometric dual-mode detection of aniline pollutants based on spiropyran derivatives. *RSC Adv.* **2016**, *6*, 83312–83320. [[CrossRef](#)]
13. Petra, G.; Romana, C.K.; Maja, V.; Boris, S. Crystal Structures and Emission Properties of the BF<sub>2</sub> Complex 1-Phenyl-3-(3,5-dimethoxyphenyl)-propane-1,3-dione: Multiple Chromisms, Aggregation- or Crystallization-Induced Emission, and the Self-Assembly Effect. *J. Am. Chem. Soc.* **2014**, *136*, 7383–7394. [[CrossRef](#)]
14. Petri, A.T.; Jouko, J.V.; Sirpa, P. Advanced material and approach for metal ions removal from aqueous solutions. *Sci. Rep.* **2015**, *5*, 8992. [[CrossRef](#)]
15. Wei, H.B.; Zhao, Z.F.; Wei, C.; Yu, G.; Liu, Z.W.; Zhang, B.; Bian, J.; Bian, Z.Q.; Huang, C.H. Antiphotobleaching: A Type of Structurally Rigid Chromophore Ready for Constructing Highly Luminescent and Highly Photostable Europium Complexes. *Adv. Funct. Mater.* **2016**, *26*, 2085–2096. [[CrossRef](#)]
16. Dennison, G.H.; Johnston, M.R. Mechanistic Insights into the Luminescent Sensing of Organophosphorus Chemical Warfare Agents and Simulants Using Trivalent Lanthanide Complexes. *Chem. Eur. J.* **2015**, *21*, 6328–6338. [[CrossRef](#)] [[PubMed](#)]
17. Azzazy, H.M.; Mansour, M.M.; Kazmierczak, S.C. From diagnostics to therapy: Prospects of quantum dots. *Clin. Biochem.* **2007**, *40*, 917–927. [[CrossRef](#)] [[PubMed](#)]
18. Cui, Y.; Song, R.; Yu, J.; Liu, M.; Wang, Z.; Wu, C.; Yang, Y.; Wang, Z.; Chen, B.; Qian, G. Dual-Emitting MOF  $\supset$   $\cap$  Dye Composite for Ratiometric Temperature Sensing. *Adv. Mater.* **2015**, *27*, 1420–1425. [[CrossRef](#)] [[PubMed](#)]
19. Pal, S.; Chatterjee, N.; Bharadwaj, P.K. Selectively sensing first-row transition metal ions through fluorescence enhancement. *RSC Adv.* **2014**, *4*, 26585–26620. [[CrossRef](#)]
20. Li, D.; Zhou, M.; Xie, L.; Yu, X.; Yu, Y.; Ai, H.; Tang, S. Synergism of pentaerythritol-zinc with  $\beta$ -diketone and calcium stearate in poly(vinyl chloride) thermal stability. *Polym. J.* **2013**, *45*, 775–782. [[CrossRef](#)]
21. Gao, B.; Chen, L.; Chen, T. Effect of electron-donating substituent groups on aromatic ring on photoluminescence properties of complexes of benzoic acid-functionalized polysulfone with Eu(III) ions. *Phys. Chem. Chem. Phys.* **2015**, *17*, 25322–25332. [[CrossRef](#)] [[PubMed](#)]
22. Reis, S.G.; Briganti, M.; Martins, D.O.; Akpınar, H.; Calancea, S.; Guedes, G.P.; Soriano, S.; Andruh, M.; Cassaro, R.A.A.; Lahti, P.M.; et al. First coordination compounds based on a bis-(imino nitroxide) biradical and 4f metal ions: synthesis, crystal structures and magnetic properties. *Dalton Trans.* **2016**, *45*, 2936–2944. [[CrossRef](#)] [[PubMed](#)]
23. Sinha, S.; Chowdhury, B.; Ghosh, P. A Highly Sensitive ESIPT-Based Ratiometric Fluorescence Sensor for Selective Detection of Al<sup>3+</sup>. *Inorg. Chem.* **2016**, *55*, 9212–9220. [[CrossRef](#)] [[PubMed](#)]

24. Baig, M.M.F.; Chen, C.T.; Chen, Y.C. Photoluminescence Determination of Aluminum Using Glutathione-Capped Gold Nanoclusters. *Anal. Lett.* **2016**, *14*, 2246–2258. [[CrossRef](#)]
25. Chen, W.W.; Jia, Y.X.; Feng, Y.; Zheng, W.S.; Wang, W.; Jiang, X.Y. Colorimetric detection of Al (III) in vermicelli samples based on ionic liquid group coated gold nanoparticles. *RSC Adv.* **2015**, *5*, 62260–62264. [[CrossRef](#)]
26. Miura, Y.; Hiraiwa, M.N.; Ito, T.; Itonaga, T.; Watanabe, Y.; Okabe, S. Bacterial community structures in MBRs treating municipal wastewater: Relationship between community stability and reactor performance. *Water Res.* **2007**, *41*, 627–637. [[CrossRef](#)] [[PubMed](#)]
27. APEX2, version 2009.9; Bruker AXS Inc.: Tokyo, Japan, 2009.
28. SAINT, version 7.68A; Bruker AXS Inc.: Tokyo, Japan, 2009.
29. Sheldrick, G.M. A short history of SHELX. *Acta Crystallogr. A* **2008**, *64*, 112–122. [[CrossRef](#)] [[PubMed](#)]
30. Frisch, M.-J.; Trucks, G.-W.; Schlegel, H.-B.; Scuseria, G.-E.; Robb, M.-A.; Cheeseman, J.-R.; Montgomery, J.-A., Jr.; Vreven, T.; Kudin, K.-N.; Burant, J.-C.; et al. *Gaussian 03Revision C.01*; Gaussian Inc.: Wallingford, CT, USA, 2004.
31. Zhang, J.; Li, B.; Zhang, L.; Jiang, H. An optical sensor for Cu (II) detection with upconverting luminescent nanoparticles as an excitation source. *Chem. Commun.* **2012**, *48*, 4860–4862. [[CrossRef](#)] [[PubMed](#)]
32. Lee, M.H.; Van Giap, T.; Kim, S.H.; Lee, Y.H. A novel strategy to selectively detect Fe (III) in aqueous media driven by hydrolysis of a rhodamine 6G Schiff base. *Chem. Commun.* **2010**, *46*, 1407–1409. [[CrossRef](#)] [[PubMed](#)]



© 2017 by the authors. Licensee MDPI, Basel, Switzerland. This article is an open access article distributed under the terms and conditions of the Creative Commons Attribution (CC BY) license (<http://creativecommons.org/licenses/by/4.0/>).